Journal of Cleaner Production xxx (xxxx) xxx

Contents lists available at ScienceDirect

Journal of Cleaner Production

journal homepage: www.elsevier.com/locate/jclepro

Exploring the sustainable production of ammonia by recycling N and H in biological residues: Evolution of fuel-N during glutamic acid gasification

Noemí Gil-Lalaguna [a], Zainab Afailal [a], María Aznar [c], Isabel Fonts [a, b, *]

[a] Thermochemical Processes Group, Aragon Institute for Engineering Research (I3A), Chemical and Environmental Engineering Department, University of Zaragoza, C/ Mariano Esquillor s/n, 50.018, Zaragoza, Spain
[b] Chemical and Environmental Department, Centro Universitario de la Defensa, Academia General Militar, Ctra. Huesca s/n, 50.090, Zaragoza, Spain
[c] Department of Mechanical Engineering, University of Zaragoza, María de Luna s/n, 50.018, Zaragoza, Spain

ARTICLE INFO

Article history:
Received 24 April 2020
Received in revised form
6 September 2020
Accepted 26 September 2020
Available online xxx

Handling Editor: Cecilia Maria Villas Bôas de Almeida

Keywords:
Sewage sludge
Meat and bone meal
Glutamic acid
Gasification
Fuel-N
Sustainable ammonia

ABSTRACT

In this work, the recycling of nitrogen and hydrogen from nitrogen-rich (N-rich) biological residues via autothermal gasification has been proposed as a process suitable for the sustainable production of ammonia (NH_3). Two N-rich biological residues, sewage sludge and meat and bone meal, were used and analyzed in this work and glutamic acid was selected as the model compound of the protein-fuel-N in these residues. Glutamic acid gasification experiments were carried out in order to study the effect of temperature (800–900 °C) and steam-to-carbon ratio (0.5–1.0 g g^{-1}) on the conversion of fuel-N into the most typical N-containing gasification products: NH_3, molecular nitrogen (N_2), hydrogen cyanide (HCN), nitrogen monoxide (NO), tar-N and char-N. Sewage sludge and meat and bone meal were also gasified under selected operating conditions with the main aim of assessing the NH_3 production. The most abundant N-containing compounds obtained in the gasification of glutamic acid were NH_3 (35–51% over fuel-N) and N_2 (45–63% over fuel-N). The highest conversion of fuel-N to NH_3–N in the glutamic acid gasification experiments (51%) was obtained at the lowest temperature (800 °C) and the lowest S/C ratio (0.5 g g^{-1}). The increase in the temperature caused a decrease in the yield of NH_3, as a consequence of its decomposition into N_2. A similar fuel-N distribution was found when sewage sludge and meat and bone meal were gasified, obtaining joint yields of HCN–N, NO–N, tar-N and char-N lower than 5%, and being NH_3–N (30–67%) and N_2–N (28–68%) the majority products. The yields of NH_3–N obtained from glutamic acid (51%), sewage sludge (30%), and meat and bone meal (67%) under the same gasification operating conditions were significantly different. These differences were attributed to the catalytic effect of the metals present in these residues and point to the need to optimize the operating conditions specifically for each residue. In summary, gasification of sewage sludge and meat and bone meal may be able to produce around 10% of the NH_3 produced annually in Europe and between 102 and 262 GJ·ton^{-1} NH_3 thanks to the combustion of the syngas generated.

1. Introduction

In the first section of the introduction, the environmental challenges of the industrial ammonia synthesis process and the different alternatives proposed in the literature are commented. The second section presents the proposed process and its novelty.

1.1. Environmental challenges of the industrial ammonia synthesis process

Ammonia (NH_3) is a commodity chemical absolutely necessary for achieving high levels of agriculture production. In fact, NH_3 is one of the most highly produced inorganic chemicals, with a current annual production rate of around 13.5 million tons (NH_3–N) for the European Union in 2018 (Eurostat, 2020) and of around 150 million tons worldwide in 2017 (U.S.G.S., 2018), of which around

* Corresponding author. Thermochemical Processes Group, Aragon Institute for Engineering Research (I3A), Chemical and Environmental Engineering Department, University of Zaragoza, C/ Mariano Esquillor s/n, 50.018, Zaragoza, Spain.
E-mail address: isabelfo@unizar.es (I. Fonts).

https://doi.org/10.1016/j.jclepro.2020.124417
0959-6526/

85% is used for the production of synthetic fertilizers. NH_3 is industrially synthesized by the Haber-Bosch process, which is based on a reversible chemical reaction in which the stable atmospheric nitrogen (N_2) reacts with hydrogen (H_2), mainly obtained by natural gas steam reforming, in a catalyst bed at high pressure (100–300 atm) and temperature (400–500 °C) to give NH_3 (N_2 (g) + 3H_2 (g) ⇆ 2 NH_3 (g) + heat). In terms of energy consumption, industrial NH_3 synthesis is the most energy demanding industrial process for the production of chemicals with an annual global consumption of $2.5 \cdot 10^6$ TJ (Brunning, 2019) and around 3–5% of the total natural gas output (Patil et al., 2015), both due to the production of H_2 from fossil fuels. Best available techniques for NH_3 synthesis in existing industrial plants reach energy consumptions as low as 28 GJ ton^{-1} NH_3 (Rafiqul et al., 2005). This process also accounts for roughly 1% of global annual CO_2 emissions, more than any other industrial chemical-making reaction (Boerner, 2019). Consequently, according to experts, there is an urgent need for alternative and more sustainable processes for NH_3 production (Baltrusaitis, 2017). The Haber-Bosch process also has environmental drawbacks because of the excessive fixation of the stable atmospheric N_2. The huge impact of anthropogenic activities on the earth's nitrogen budget has destabilized the equilibrium state in the biogeochemical nitrogen (N) cycle and has increased the net content of reactive N-containing compounds in soil, water and the atmosphere (Rockström et al., 2009a). According to Rockström et al. (2009b), humanity has already transgressed three planetary boundaries which, ordered according to their hazard level, are biodiversity loss, imbalance in the N biogeochemical cycle and climate change. These experts estimated that the amount of N_2 removed from the atmosphere for human use should be reduced from 121 million tons (similar value to current consumption) to 35 million tons per year in order to recover a sustainable level in the biogeochemical N-cycle (Rockström et al., 2013). This supports the necessity of developing a sustainable alternative for NH_3 production, which should involve not only the use of renewable hydrogen (H) and the reduction of the energy consumption, but also the use of a reactive N source instead of stable atmospheric N_2.

More sustainable alternatives to the Haber-Bosch process joint to H_2 production from fossil fuels have been the subject of research for the last decade. There is an offshoot focused on the integration of alternative H_2 production processes with the synthesis of NH_3 via Haber-Bosch, standing out those based on biomass gasification (Andersson and Lundgren, 2014), on chemical looping (Nurdiawati et al., 2019) and on water electrolysis powered by solar energy (Wang et al., 2018). Other proposed strategies do not imply the synthesis of NH_3 via the Haber Bosch process but using different reactions such as, catalytic electrochemical synthesis from N_2 and H_2O over metal hydroxides (Qiao et al., 2020), metal oxides, metal nitrides and metal carbides (Cui et al., 2018) or the steam-hydrolysis of metallic nitrides such as CrN (Michalsky and Pfromm, 2011) and AlN using concentrated thermal radiation (Gálvez et al., 2009) or by providing energy through biomass combustion (Juangsa and Aziz, 2019). The commercial development of all these alternatives could bring advantages regarding the energetic balance of the processes in comparison with the conventional Haber-Bosch with H_2 production from fossil fuels, but not from the point of view of the fixation of the stable atmospheric N_2.

1.2. Novel process for producing sustainable NH_3 by recycling N and H from N-rich biological residues

Drawing an analogy with lignocellulosic biomass as a source of renewable carbon (C) for the production of bioenergy and bioproducts, N-rich biological residues, such as sewage sludge, meat and bone meal or manure, could be a possible source of both renewable H and reactive N. The direct application of these residues as agricultural fertilizer is limited by the nature of some of their constituents, such as heavy metals and pathogens, as well as their increasing, centralized and continuous production. Moreover, it is worth noting that the production of these three residues is not negligible. For instance, according to European authorities, around 18 Mt y^{-1} of animal fat and meat industry by-products arise annually in the European Union (EU) from slaughterhouses, dairies and plants producing food for human consumption (Jędrejek et al., 2016). Eurostat database shows a European average production of dry sewage sludge of around 10 Mt y^{-1} in 2018 (Eurostat, 2019).

As regards a possible process for N-recovery in the form of NH_3, it is known that during gasification, the nitrogen contained in the raw material (fuel-N) is mainly released as NH_3, hydrogen cyanide (HCN), N_2, tar-N and char-N (Leppalahti and Koljonen, 1995). To date, in view of the energetic and synthesis applications of gasification gas, NH_3 and HCN have been considered as pollutants and undesirable compounds because of being precursors of NOx in combustion and poisons for the catalytic post-upgrading of syngas. In order to minimize the formation of such compounds, various aspects have been studied related to the evolution of fuel-N during the gasification of lignocellulosic biomass and, to a lesser extent, of N-rich biological residues (see Table 1). The mechanism by which fuel-N evolves during gasification depends on the N-functionality (Leppalahti and Koljonen, 1995). In lignocellulosic biomass and other biological raw materials, whose major N-functionality is in the form of proteins, fuel-N is released during the pyrolysis stage (Leppalahti and Koljonen, 1995), but also during the char gasification and tar cracking reactions (Broer and Brown, 2015). NH_3, HCN and tar-N are the main volatile-N species involved in the process. During biomass pyrolysis, the partitioning of fuel-N between volatiles-N and char-N depends on the final temperature and on the char-N functionality, which changes during the pyrolysis process (Wei et al., 2015). Apart from pyrolysis, the conversion of char-N and tar-N to gaseous species such as NH_3 increased with equivalence ratio (O_2 presence) (Broer and Brown, 2016). According to Tian et al. (2007), thermal-cracking/steam reforming of volatile-N constitutes also an important route for NH_3 production. Lastly, secondary gas phase reactions also influence the final distribution of fuel-N among the N-containing products (Liu and Gibbs, 2003).

The extent of each of the aforementioned reactions may vary significantly with the change in the operating conditions or even by the effect of other raw material constituents, causing variations in the final distribution of the N-containing products obtained from the gasification process. Table 1 shows the fuel-N distribution obtained in previous research works dealing with gasification of different types of biomass. As can be observed in Table 1, there is great variability in the fuel-N distributions reported in the literature. It is possible to find works in which the major product is either N_2 (Aznar et al., 2009; Broer and Brown, 2016; Zhou et al., 2000) or NH_3 (de Jong et al., 2003; Kurkela and Stahlberg, 1992; Zhou et al., 2000). As regards fuel-N conversion to NH_3–N, values from 10.5% to 63.5% have been obtained in the gasification of Leucaena in a fluidized bed reactor at 950 °C and 750 °C (Zhou et al., 2000), values of around 57% during the gasification of woody biomass at 850 °C (Jeremias et al., 2014) and around 19–33% during the gasification of pine (Abdoulmoumine et al., 2014). Table 1 also shows that the conversions of fuel-N to other N-containing products also have very different values ranging from 1.2 to 34% for char-N, from 5.9 to 38% for tar-N and from 0 to 20% for HCN–N. There are only few works in which tar-N compounds have been characterized. In these works, tar-N compounds have been analyzed only qualitatively (Aznar et al., 2009; Gil-Lalaguna et al., 2014) or quantitatively but providing the quantification of only a very small number of tar compounds (Yu et al., 2007). There is some controversy in the

Table 1
Summary of fuel-N distribution (%) results in biomass gasification studies reported in the literature.

Raw material	N in raw material (daf %)	T (°C)	ER	Gasifying agent	S/C mass ratio	Bed material	char-N (%)	tar-N (%)	HCN–N (%)	NH_3–N (%)	N_2 (%)
Lignocellulosic biomass											
Switchgrass[a]	0.05	750	0–0.40	O_2+CO_2	–	Silica sand	11–34	21–38	9.8	6–15	11–40
Cedar wood[b]	0.10	850	0–0.2	O_2+H_2O	0–2	No bed, updraft gasifier	–	–	<0.2	6–55	–
Wood[c]	0.19	850	0.2	O_2+H_2O; O_2+CO_2; O_2+ CO_2 + H_2O	0.2–1.8	Sand; Sand/dolomite mixtures	–	–	–	43–57	–
Cane trash[d]	0.36	600–800	–	H_2O	–	Zircon sand	–	–	8–20	20–50	–
Pine[e]	0.44	790–1078	0.15–0.35	O_2	–	sand	–	–	1.6–2.8	19–33	–
Switchgrass[f]	0.53	700–900	0.20–0.40	O_2+H_2O	1[k]	Silica sand	–	–	2.6–14	32–50	–
Miscanthus[g]	0.7	700–800	0–0.25	Air	–	Alumina	14–21	–	<0.06	22.4–46.0	–
Leucaena[h]	3.05	700–900	0.18–0.32	O_2+Ar	–	Alumina	1.2–7.7	–	<0.11	10.5–63.5	38.6–88.7
N-rich biological residues (non-lignocellulosic)											
Cattle manure[i]	2.6	800	0	H_2O	1.5	Silica sand; Limestone; Kaolin	–	–	–	37	–
Pig manure[i]	3.1	800	0	H_2O	1.5	Silica sand; Limestone; Kaolin	–	–	–	33	–
Sewage sludge[i]	7.1	800	0	H_2O	1.5	Silica sand; Limestone; Kaolin	–	–	–	48	–
Sewage sludge[j]	7.55	850	0.21–0.30	O_2+Ar, Air	–	Ash; Sewage sludge ash	1.4–8.5	5.9–20.6	0.7–1.6	13.2–28.1	47.4–74.7
Sewage sludge[d]	18.6	700	–	H_2O	–	Zircon sand	–	–	–	30–45	–

[a] (Broer and Brown, 2016).
[b] (Aljbour and Kawamoto, 2013).
[c] (Jeremias et al., 2014).
[d] (Tian et al., 2007).
[e] (Abdoulmoumine et al., 2014).
[f] (Broer et al., 2015).
[g] (Vriesman et al., 2000).
[h] (Zhou et al., 2000).
[i] (Schweitzer et al., 2018).
[j] (Aznar et al., 2009).
[k] Steam to O_2 mass ratio.

literature about the influence of temperature and the equivalence ratio (ER) on the conversion of fuel-N to NH_3. For example, while some authors claim that as the gasification temperature increases, both the conversion of fuel-N to NH_3–N and the concentration of NH_3 in the gasification gas decrease (Abdoulmoumine et al., 2014; Zhou et al., 2000), some others have observed the opposite trend (Broer and Brown, 2015; Vriesman et al., 2000). The equivalence ratio also has an ambiguous effect on the yield of NH_3, since different studies report a positive effect (Broer and Brown, 2016; Vriesman et al., 2000), a negative effect (Broer et al., 2015) or even a non-significant effect (Abdoulmoumine et al., 2014; Aznar et al., 2009). The effect of other operating conditions on the conversion of fuel-N to NH_3–N seems to be clearer. For example, both the use of steam as gasifying agent (Cao et al., 2015; Chang et al., 2003) and the use of dolomite as bed material (Cao et al., 2015; Corella et al., 2004; Jeremias et al., 2014) seem to have a positive effect.

Most of the fuel-N in lignocellulosic biomass and biological residues is in the form of proteins, peptides and amino acids, usually referred to as the protein fraction. The protein fraction is the main source of NH_3 during gasification. Therefore, the use of a protein or amino acid model compound could be very useful for a first approach to evaluating the effect of the operating conditions on the chemistry involved in the fuel-N conversion during the gasification of N-rich biological residues, cutting out the effect that the other constituents of the residues may have. Model proteins (Hansson et al., 2004) and some selected amino acids have previously been used to study the evolution of NOx precursors in the pyrolysis of biomass (Ren and Zhao, 2015).

Against this background, the final goal of the research work presented in this paper is to evaluate the sustainable production of NH_3 via gasification of N-rich biological residues as a possible way to deal with two environmental issues: (i) the high demand of resources and the excessive fixation of atmospheric N_2 for the current NH_3 production process and (ii) the management of N-rich biological residues in an environmentally-friendly way. For this purpose, the fuel-N partitioning into NH_3–N, HCN–N, NO–N, char-N and tar-N has been evaluated when gasifying a model amino acid compound (glutamic acid) at different gasification operating conditions (variation of temperature and steam-to-carbon mass ratio). An extensive characterization of the tar product composition was also performed. Sewage sludge (SS) and meat and bone meal (MBM) gasification experiments have been carried out under selected operating conditions with the main aim of assessing the possible production of NH_3 from these residues. These results have been compared with those found in the literature in order to help to figure out which factors/reactions determine the fuel-N distribution.

2. Experimental

This section shows the selection of the model compound and an in depth characterization of the selected model compound and the

two N-rich biological residues used in the gasification experiments. Next, the experimental setup, procedure and planning are exposed.

2.1. Characterization of N-rich biological residues: model compound selection

Two N-rich biological wastes, MBM and SS, were characterized in order to choose a representative N-protein model compound. The nitrogen content in these wastes was 9.9 wt % (MBM) and 4.7 wt % (SS) (analyzed with an elemental analyzer LECO CHN628 – 628S).

2.1.1. Amino acids analysis (protein hydrolysis)

As mentioned above, most of the fuel-N of these types of waste comes from their protein fraction. The total protein fraction in these three wastes, which includes free amino acids, amino acids in peptides and amino acids in proteins, was measured at the Biological Research Center (CSIC, Spain). Samples were analyzed in duplicate in an ionic chromatograph (Biochrom 30) after hydrolysis. A commercial standard mixture of 17 amino acids was used for calibration: aspartic acid (Asp), threonine (Thr), serine (Ser), glutamic acid (Glu), proline (Pro), glycine (Gly), alanine (Ala), cysteine (Cys), valine (Val), methionine (Met), isoleucine (Ile), leucine (Leu), tyrosine (tyr), phenilaniline (Phe), histidine (His), lysine (Lys) and arginine (Arg).

The total contents of amino acids in MBM and SS (calculated as the sum of the individual concentrations, which are shown in Fig. 1) were 49.8 wt % and 20.8 wt %. The data from the amino acid analyses enabled us to determine the percentage of fuel-N in the form of amino acid-N, that is to say protein-fuel-N, in MBM and SS. These were 78.0 wt % and 73.1 wt %. Glutamic acid (GLU) was the most abundant amino acid in MBM, and the second most abundant in SS. In view of these results, GLU was selected as the N-model compound to be used as raw material in the parametric gasification study.

2.2. Characterization of the raw materials used in the gasification experiments

Gasification experiments were carried out with three different raw materials. Firstly, a parametric gasification study was conducted with GLU in order to evaluate the impact of some operating conditions. Then, SS and MBM were also gasified with the main aim of assessing the potential production of NH_3 from real residues.

Analytical grade L-glutamic acid powder (purity > 99 wt %) was purchased from Sigma Aldrich, while MBM was supplied by a Spanish animal by-products treatment company, where MBM were sterilized in an autoclave at 133 °C and 3 bar during 20 min, and SS came from a Spanish wastewater treatment plant, where SS was anaerobically digested and thermally dried.

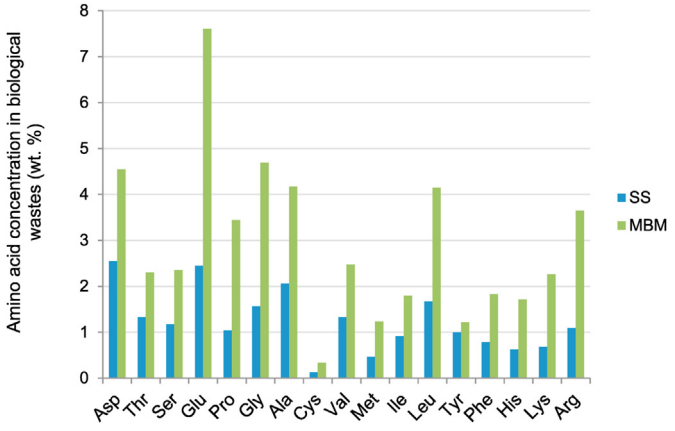

Fig. 1. Content of amino acids in sewage sludge (SS) and meat and bone meal (MBM).

The moisture and ash content analyses of GLU, SS and MBM were determined in accordance with EN ISO 18134:2015 and EN ISO 18122:2015. The elemental analyses were experimentally performed using a LECO CHN 628 Series elemental analyzer. The higher heating values of the three raw materials were determined using a C2000 IKA bomb calorimeter. The results obtained in these analyses are shown in Table 2. The compositions of the ash in the MBM and SS were determined by inductively coupled plasma optical emission spectroscopy (ICP-OES) and can be seen in Table 2.

Taking into account the amount of N and H fed to the system and the relation N:H in NH_3, N is limiting in comparison with H. For this reason, the efficiency of the process in terms of NH_3 formation can be measured by the percentage of fuel-N that ends as NH_3–N.The model amino acid (GLU) was further characterized by thermogravimetric analysis (TGA) and X-ray photoelectron spectroscopy (XPS). Pyrolysis of GLU at 900 °C under inert atmosphere was carried out in a thermobalance (Netzsch STA 449 F1 Jupiter) and the nitrogen content of the solid product obtained (GLU_PIR900) was determined to aim at following the evolution of the fuel-N remaining in the solid after thermal devolatilization (without taking place any other reaction). In this case, the conversion of fuel-N to char-N at 900 °C reached 25%, so the rest of the fuel-N (75%) was released in the form of volatiles (gaseous species and tar). On the other hand, the XPS analysis allowed determining the evolution of the N-functionality in GLU after such pyrolysis process. More information about these procedures and results are detailed in the Supplementary Information Section: Thermogravimetric and XPS results of GLU pyrolysis.

2.3. Gasification setup

The gasification runs were conducted in a gasification setup equipped with a laboratory-scale fluidized bed reactor operating at atmospheric pressure. A schematic diagram of the setup is shown in Fig. 2, and more details about the reactor specifications can be found elsewhere (Gil-Lalaguna et al., 2014).

Significant operational problems were found when attempting to continuously feed the GLU powder into the reactor with a screw

Table 2
Composition of the three raw materials (as received basis).

	GLU	MBM	SS
Carbon (wt. %)	41.0	45.34	27.85
Hydrogen (wt. %)[a]	6.0	6.65	4.89
Nitrogen (wt. %)	9.5	9.9	4.7
Oxygen (wt. %)[b]	43.2	20.14	20.84
Sulfur (wt. %)	0.0	0.54	1.41
Ash (wt. %)	<0.01	17.40	40.36
Moisture (wt. %)	0.3	4.64	7.66
Al_2O_3 (wt%, in ash)		1.1	9.68
CaO (wt%, in ash)		32.6	9.09
Fe_2O_3 (wt%, in ash)		1.4	26.62
K_2O (wt%, in ash)		6.2	1.68
MgO (wt%, in ash)		3.5	2.80
Na_2O (wt%, in ash)		6.1	0.60
SiO_2 (wt%, in ash)		6.8	26.07
TiO_2 (wt%, in ash)		0.1	0.67
P_2O_5 (wt%, in ash)		35.2	7.1
HHV ($MJ \cdot kg^{-1}$)	14.35	20.0	12.4

[a] The percentage of hydrogen includes hydrogen from moisture.
[b] Oxygen was calculated by difference as O (wt. %) = 100 - C (wt. %) - H (wt. %) - N (wt. %) – S (wt. %) - Ash(wt. %).

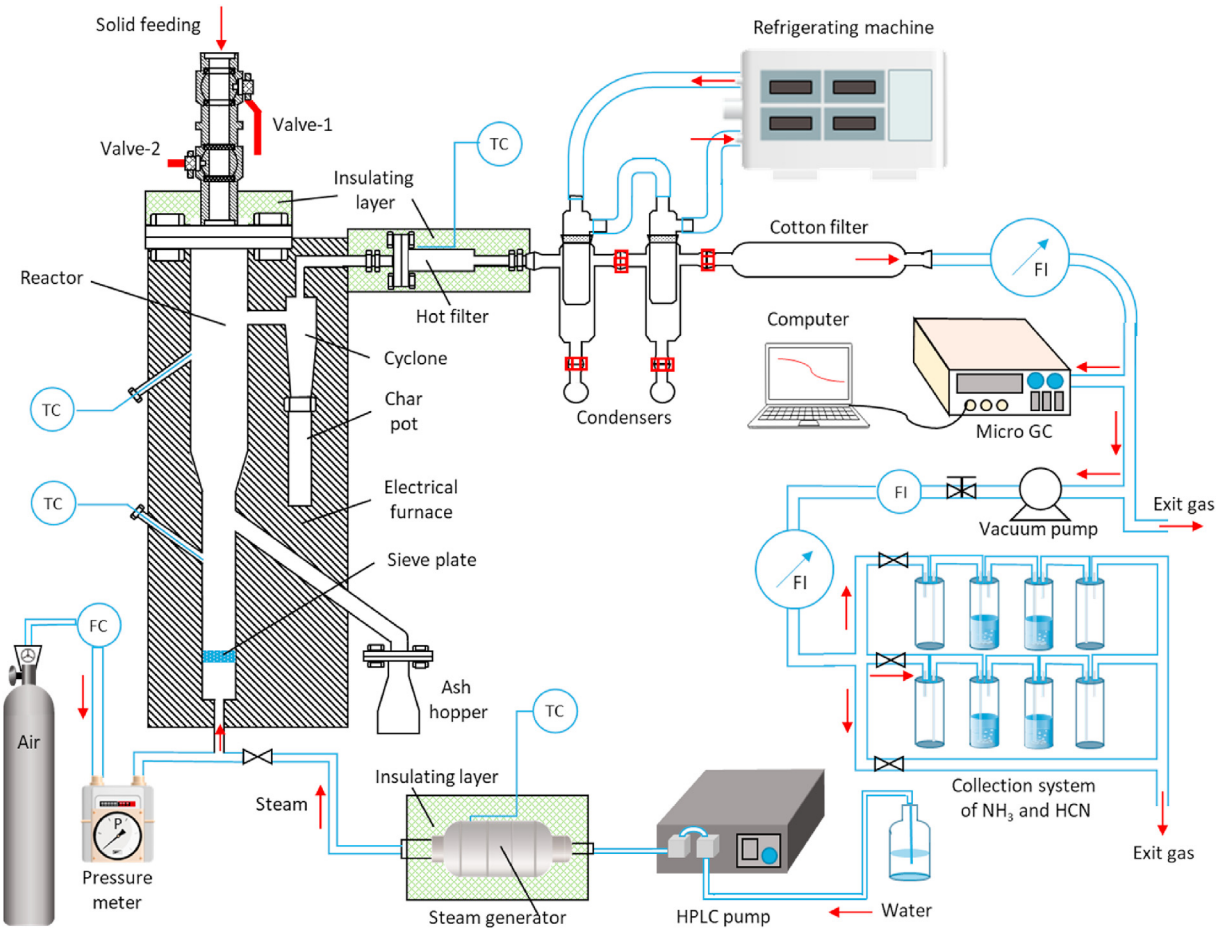

Fig. 2. Schematic diagram of gasification setup (FC: mass flow controller; FI: volumetric flow indicator; TC: temperature controller).

feeder. The material swelled when heated, causing plugging problems in the reactor inlet tube. The cooling of the tube was not enough to prevent this phenomenon. Given these operational problems, the continuous feed of GLU into the gasifier by means of a screw feeder was ruled out. The feeder was replaced by a double valve feeding system placed at the upper part of the reactor. Small tablets of GLU (1.5 cm diameter and 2–3 mm thickness) were prepared with a pressing machine. During the gasification experiments, these tablets were manually fed in pulses of 2.5 g per minute (test duration of 60 min) through the double valve system at the top of the reactor. SS and MBM were fed by the upper double valve system in the same way as GLU in order not to influence the gasification performance. Small tablets of MBM (1.5 cm diameter and 2–3 mm thickness) were also prepared for feeding to the reactor, while SS was fed as received, that is in spherical shape particles (4–5 mm).

The gasifying/fluidizing mixture, composed of air and steam, entered the reactor below the distributor plate and passed through the dolomite bed (~100 g, d_p = 350–500 μm). Details about the feeding systems for air and steam are explained elsewhere (Gil-Lalaguna et al., 2014).

After leaving the reactor, particulate matter swept by the gas flow was sequentially removed in a hot cyclone (at a temperature of 600–700 °C) and in a glass wool hot filter (450 °C). Tar and water, as well as part of the NH_3 and HCN generated during gasification, were collected in two condensers arranged in series and cooled at 0.5 °C with a water-recirculating chiller. After passing through the condensers, the gas was driven through a cotton filter, which retained small aerosols swept up by the gas. The volume of particle- and tar-free gas was continuously measured by a volumetric meter and its composition was analyzed on-line using a micro gas chromatograph (Agilent 3000-A), which determined the volume percentages of H_2, N_2, O_2, CO, CO_2, CH_4, C_2H_4, C_2H_6, C_2H_2 and H_2S. Then, around 1 $m^3(STP)\cdot min^{-1}$ of the gas stream was drawn alternatively into one of the two absorption traps (absorption bubblers) arranged in parallel, one for NH_3 and the other for HCN, in order to be sure that all the NH_3 and the HCN from the gas samples were collected. The total volume of gas drawn through each absorption trap was measured and recorded. Sampling and analysis of the NH_3 and HCN collected in the condensers and in the absorption bubblers is explained in greater depth elsewhere (Aznar et al., 2009). At the gas exit, some producer gas was also collected in a Tedlar gas sampling bag for off-line determination of NO by non-dispersive infrared analysis (Advance Optima Infrared Analyzer ModuleUras 14).

Both char and condensed liquid mass yields were determined gravimetrically by weight difference of the corresponding vessels used for their collection. In the case of GLU experiments, the elemental analysis of the solid product was only undertaken on the fraction recovered in the cyclone, since the solid remaining in the bed was essentially pure dolomite, while the solid fraction collected in the hot filter was discarded for the analysis as it could be polluted with adsorbed tar. In the case of SS and MBM, it was possible to recover some remains of ash/char from the bed to be analyzed. A known mass of methanol was used to wash the condensers and recover the tar. Water content of the mixture was analyzed by Karl Fischer titration, obtaining a gravimetric measure of tar by difference.

Tar composition was qualitatively and quantitatively analyzed by gas chromatography with mass spectroscopy and flame ionization detectors (GC-MS/FID). In the Supplementary Information section, Table S1 summarizes the operating parameters for the GC-MS/FID analyses. NIST MS Search Program 2.2 was used for the identification of the compounds with the MS signal. In addition, the FID signal was calibrated for tar quantification. A commercial standard solution of 16 polycyclic aromatic hydrocarbons (PAH) (PAH Mix 63, 1000 μg mL^{-1} in toluene, purchased from the Dr. Ehrenstorfer company) and 10 dilutions of it (3–500 μg mL^{-1} of each compound) were used for calibrating naphthalene and heavier PAH. Moreover, 5 standards of N-containing tar compounds (pyridine, pyrrole, benzonitrile, indole, quinoline) were prepared (80–1500 μg mL^{-1} of each compound) from high-purity chemicals, using a mixture of methanol-dichloromethane (1:1 vol) as solvent. The FID response factors of the compounds that were identified by GC-MS, but not calibrated as standards, were calculated from the response factor of the most similar standard used, applying to it a correction factor following the methodology based on the Effective Carbon Numbers (ECN) (see the procedure description in the Supplementary Information). ECN theoretical values were calculated following procedures described in the literature (contribution of functional groups to ECN) (Scanlon and Willis, 1985) or directly obtained from the bibliography in the case of some specific compounds (Jorgensen et al., 1990) (see procedure in the Supplementary Information and ECN values in Table S2).

2.4. Operating conditions of the gasification experiments

GLU gasification experiments were planned following a 2^k factorial design aiming at evaluating the impact of the temperature (*T*) and the steam-to-carbon mass ratio (*S/C*) on fuel-N partitioning: char-N, tar-N and gas-N in the form of NH_3, HCN and NO. The operating conditions in the GLU, SS and MBM gasification experiments are summarized in Tables 3 and 6.

As Broer and Brown (2016) highlighted, most of the works that deal with the chemistry of fuel-N during biomass gasification, especially at atmospheric pressure, study the effect of the *T* and the equivalence ratio *(ER)* as independent variables, although they are actually dependent in industrial-scale gasification plants. For this reason, *T* and *ER* have been evaluated as dependent variables in the present work. For this purpose, the *ER* required for autothermal operation under each pair of *T-S/C* values set as operating conditions has been calculated with a non-stoichiometric thermodynamic model. As chemical equilibrium of the gasification reaction is expected to be closely approached at high temperatures, gasification can be modeled with reasonable accuracy using thermodynamic equilibrium models. HSC 9.4.1 software for Excel add-in has been used to calculate the *ER* required for conducting each experimental run in autothermal conditions. The calculation procedure of the HSC 9.4.1 software is based on (i) minimization of the Gibbs free energy of the system and (ii) atomic mass balance equations. Moreover, (iii) an energy balance has been included in the model by the authors of this work, assuming heat losses of 5%, in order to determine the air input requirement for autothermic conditions. The *ER* calculated and used in each experiment can be observed in Tables 3 and 6

Statistical analysis of variance (ANOVA) with a confidence level of 90% was performed to verify the statistical significance of the observed effects and interactions of the two factors. One-way ANOVA coded models have been tested to fit the experimental data. Interpretation of the coded models from one-way ANOVA is explained in depth elsewhere (Fonts et al., 2008).

3. Results

Table 3 summarizes the main operating conditions and the fuel-N distribution obtained in the gasification of GLU. The mass balance in the gasification tests varied from 93 to 100% and the individual atomic balances of C, H, N and O were also close to 100% (89–103%),

Table 3
Operating conditions and experimental results of fuel-N distribution in the gasification of GLU.

	Test 1	Test 2	Test 3	Test 4	Test 5, 6,7 [a]
Gasification temperature, °C	800	900	800	900	850
Steam-to-carbon ratio, $g \cdot g^{-1}$	0.5	0.5	1	1	0.75
Air feed, $g \cdot min^{-1}$	5.86	6.36	6.15	6.71	6.26
H_2O feed, $g \cdot min^{-1}$	0.505	0.505	1.018	1.018	0.761
Equivalence ratio, %	32.4	35.2	34.0	37.2	34.7
Fluidizing velocity, $m \cdot s^{-1}$ [b]	0.27	0.32	0.31	0.37	0.32
Wet gas velocity in freeboard, $m \cdot s^{-1}$	0.128	0.147	0.134	0.153	0.138 ± 0.004
Average gas residence time, s [c]	4.9	4.2	4.5	4.0	4.4
Fuel-N distribution (nitrogen yield over fed GLU-N, %)					
NH_3–N	51	35	40	40	45 ± 2
HCN–N	1.0	0.9	1.5	1.4	1.8 ± 0.1
NO–N	0.29	0.20	0.25	0.18	0.21 ± 0.04
Char-N	0.3	0.5	1.4	0.5	0.7 ± 0.1
N–N_2 (by difference)	45	63	55	57	51 ± 2
Tar-N (Total, 1 + 2)	2.14	0.50	2.04	0.75	1.31 ± 0.03
Tar-N distribution into different families (nitrogen yield over fed GLU-N, %)					
Fuel-N to heterocyclic tar-N (1)	1.77	0.40	1.74	0.62	1.09 ± 0.03
Fuel-N to pyridinic-N (1-a)	1.364	0.265	1.375	0.449	0.816 ± 0.005
Fuel-N to pyrrolic-N (1-b)	0.0311	0.0011	0.0459	0.0017	0.0064 ± 0.0009
Fuel-N to quinolinic-N (1-c)	0.17	0.07	0.11	0.09	0.13 ± 0.02
Fuel-N to indoles (1-d)	0.194	0.065	0.197	0.080	0.140 ± 0.007
Fuel-N to indolizines (1-e)	0.0115	0.0004	0.0108	0.0005	0.0026 ± 0.0001
Fuel-N to aromatic tar-N (2)	0.376	0.097	0.299	0.131	0.215 ± 0.005
Fuel-N to aromatic nitriles (2-f)	0.345	0.081	0.270	0.111	0.191 ± 0.006
Fuel-N to aromatic azides and amines (2-g)	0.031	0.016	0.029	0.020	0.024 ± 0.001

[a] Results of experiments 5, 6 and 7 are expressed as mean ± standard deviation.
[b] The fluidizing velocity only relates to the flow of the gasifying agent (air + steam) passing through the dolomite bed. This velocity was 3–6 times higher than the minimum fluidizing velocity of dolomite (350–500 μm).
[c] The residence time of gases and vapors in the reactor was calculated from the reactor volume and the gas flow data (including steam and tar vapors).

which points to good experimental procedures. Mass balances can be seen in Table S3 of the Supplementary Information.

3.1. Fuel-N distribution during glutamic acid gasification

In the current section, an overview of the fuel-N distribution obtained from the gasification of GLU is first explained. Next, the effect of the *T* and the *S/C* ratio on the fuel-N distribution and on the tar composition is discussed using the results of the ANOVA analyses.

3.1.1. General trends

Fig. 3 shows the partitioning of the fuel-N among the different N-containing products determined experimentally in the GLU gasification experiments.

The conversion of fuel-N into char-N, tar-N, NO–N, NH_3–N and HCN–N accounted for 38–55% (Fig. 3). NH_3 was the most abundant product among these N-containing compounds determined experimentally (35–51%), reaching a maximum conversion of fuel-N to NH_3–N of 51% when the GLU gasification was performed at 800 °C and with a *S/C* mass ratio of 0.5. As N is limiting in comparison with H, the yields of fuel-H (only considering H from raw materials and not from steam) to NH_3–H were of course lower (10–23%) than the ones of fuel-N to NH_3–N (35–51%).

It was attempted to calculate the molecular nitrogen (N_2) generated from the fuel-N as the difference between the mass of N_2 contained in the exit gasification gas (experimentally determined from the micro-GC and the volumetric meter data) and the mass of N_2 introduced into the fluidized bed with the air. However, the results obtained were not consistent due to the high amount of N_2 coming from the gasification agent in comparison with that formed from the raw material. Nevertheless, based on the knowledge of solid fuel-N distribution in biomass gasification processes (Aznar et al., 2009) and of the evolution of N-containing gas species according to gas-phase gasification reaction mechanisms under reducing atmosphere (Liu and Gibbs, 2003), it is expected that most of the remaining fuel-N that was unable to be properly determined experimentally was in the form of N_2. Hence, the conversion of fuel-N to N_2, obtained by difference, would be between 45 and 62%. Therefore, depending on the operating conditions tested in this gasification work, the main N-containing product could be NH_3 or N_2.

Other N-containing gases such as NO and HCN were produced at small rates, obtaining a fuel-N conversion to HCN–N between 0.9 and 1.8%, and <0.30% in the case of NO–N. In the few works in which the conversion of fuel-N to NO–N or NO_x-N has been determined (Yu et al., 2007; Zhou et al., 2000), the values obtained in all cases were also very low (<0.66%). HCN–N yields reported in the literature are in a wider range, from 0 to 20% (see Table 1).

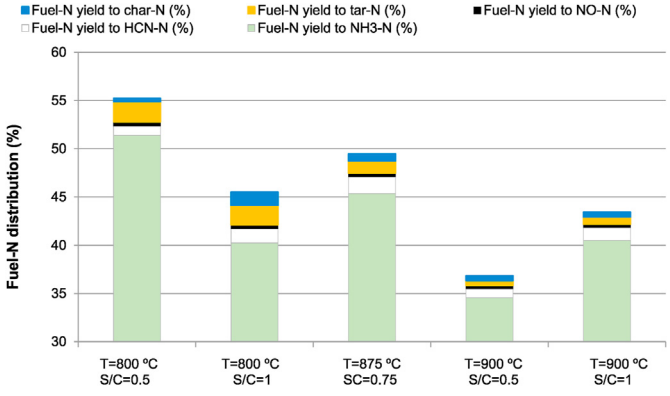

Fig. 3. Fuel-N distribution among the N-containing products determined experimentally in GLU gasification.

Char-N from GLU gasification also accounted for a low percentage of the fuel-N. Comparing the conversion of fuel-N to char-N obtained in these gasification experiments (approximately from 0.3 to 1.4%) and the yield of char-N obtained from the pyrolysis of GLU at 900 °C (25%) (see Thermogravimetric results in Supplementary Information Section), it can be said that fuel-N is released in both devolatilization reactions (pyrolysis) and char gasification reactions.

As commented before, individual species of tar generated in GLU gasification experiments were identified by GC-MS and quantified by the integration of the GC-FID signal. These tar compounds were firstly classified into N-containing tar compounds, which includes two chemical families: (1) heterocyclic tar-N compounds (N atom inside the ring) and (2) aromatic tar-N compounds (N atom outside the ring) and into N-free tar, which mainly refers to PAH (3). The (1) heterocyclic tar-N compounds can, in turn, be classified into five different types: pyridines, pyrroles, quinolones, indoles and indolizines. The (2) aromatic tar-N compounds can be classified into aromatic nitriles, and aromatic azides and amines. Table S4 in the Supplementary Information Section provides a list of the yields (over fed GLU) of individual species and Table 4 shows the yields of each one of the tar families.

As can be observed in Table 4, the total tar yield determined by GC-FID, including PAH-tar and N-containing tar, oscillated between 4.5 and 15.3 g kg^{-1} over fed GLU. Regardless of the operating conditions, N-containing tar compounds accounted for at least 75 wt % of the total tar. The fraction of N-containing tar was higher (90–93 wt %) when operating at the lowest gasification temperature (800 °C).

Regarding the distribution of fuel-N in the tar-N families, heterocyclic tar-N accounted for more than 80–85% of the total tar-N in most cases. Among heterocyclic tar-N families, pyridinic-N was the most abundant type, accounting for 66–79% of the heterocyclic tar-N.

In the few published works in which tar-N compounds are analyzed by gas chromatography, it was also found that heterocyclic tar compounds accounted for the highest percentage of the chromatographic area (Aznar et al., 2009). Specifically, Yu et al. (2007) found that pyridine was the most abundant compound in the tar mixture.

3.1.2. Effect of the operating conditions on the fuel-N distribution obtained from glutamic acid gasification

Table 5 shows the codified terms and R^2 obtained from the one-way ANOVA of the effect of the *T* and the *S/C* ratio on fuel-N distribution into the different N-containing products. R^2 is defined as the ratio between the sum of squares explained by the model and the total sum of squares. The lack of fit for all the models provided has been found to be not significant (p-value < 0.1). These models have been used for the building of interaction plots shown in Figs. 4 and 5. The model terms shown in Table 5 are usually higher for the *T* than for the *S/C* ratio, which means that the effect of *T* on the fuel-N distribution is greater than the impact of *S/C* ratio.

Fig. 4 shows the interaction plot of the effect of the *T* and the *S/C* mass ratio on the conversion of fuel-N to char-N (a), heterocyclic tar-N (b) and aromatic tar-N (c).

In some cases, the effects of the *T* and the *S/C* ratio had a mutual influence in such a way that one factor was only found to be significant at the lowest level of the other. For the lowest temperature, the conversion of fuel-N to char-N decreased as the *S/C* ratio was reduced, indicating a faster kinetic for the remaining solid-N when the gasifying medium contains a higher O_2 concentration.

Table 4
Tar yield (g tar·kg^{-1} GLU) distributed into different families.

	Test 1	Test 2	Test 3	Test 4	Test 5, 6,7[a]
Total tar (1 + 2+3) quantified by GC-FID	15.3	4.5	13.8	6.4	9.6 ± 0.5
N-containing tar (1 + 2)	13.8	3.4	12.8	5.0	8.5 ± 0.3
Heterocyclic tar-N (1)	11.1	2.7	10.7	4.0	6.9 ± 0.3
Aromatic tar-N (2)	2.74	0.70	2.14	0.95	1.54 ± 0.07
Polycyclic aromatic hydrocarbons (PAH) tar (3)	1.5	1.1	1.0	1.4	1.2 ± 0.1
Fraction of N-containing tar in total tar (wt. %)	90	76	93	78	89 ± 1

[a] Results of experiments 5, 6 and 7 are expressed as mean ± standard deviation.

Table 5
One-way ANOVA model terms for the fuel-N distribution.

Response variable	Independent term	T	S/C	T·S/C	R^2
Fuel-N to char-N (%)	0.68 (±0.18)	−0.17 (±0.18)[n.s.]	0.26 (±0.18)	−0.25 (±0.18)	0.95
Fuel-N to tar-N (%)	1.36 (±0.04)	−0.73 (±0.04)	0.037 (±0.04)	0.089 (±0.04)	0.99
Fuel-N to heterocyclic tar-N (%)	1.13 (±0.04)	−0.62 (±0.04)	0.048 (±0.04)	0.061 (±0.04)	0.99
Fuel-N to aromatic tar-N (%)	0.23 (±0.005)	−0.11 (±0.01)	−0.011 (±0.007)	0.028 (±0.007)	1.00[b]
Fuel-N to HCN−N (%)	1.18 (±0.08)	n.s.	0.24 (±0.08)	n.s.	0.92[b]
Fuel-N to NO−N (%)	0.23 (±0.03)	−0.040 (±0.035)	n.s.	n.s.	0.60[a]
Fuel-N to NH_3−N (%)	41.68 (±2.79)	−4.15 (±2.79)	−1.31 (±2.79)	4.27 (±2.79)	0.95
Fuel-N to N_2 (%)	54.88 (±2.56)	5.12 (±2.56)	0.78 (±2.56)	−4.08 (±2.56)	0.97[b]

[n.s.] not significant term.
[a] The overall mean is a better predictor of the response than the current model.
[b] Significant curvature.

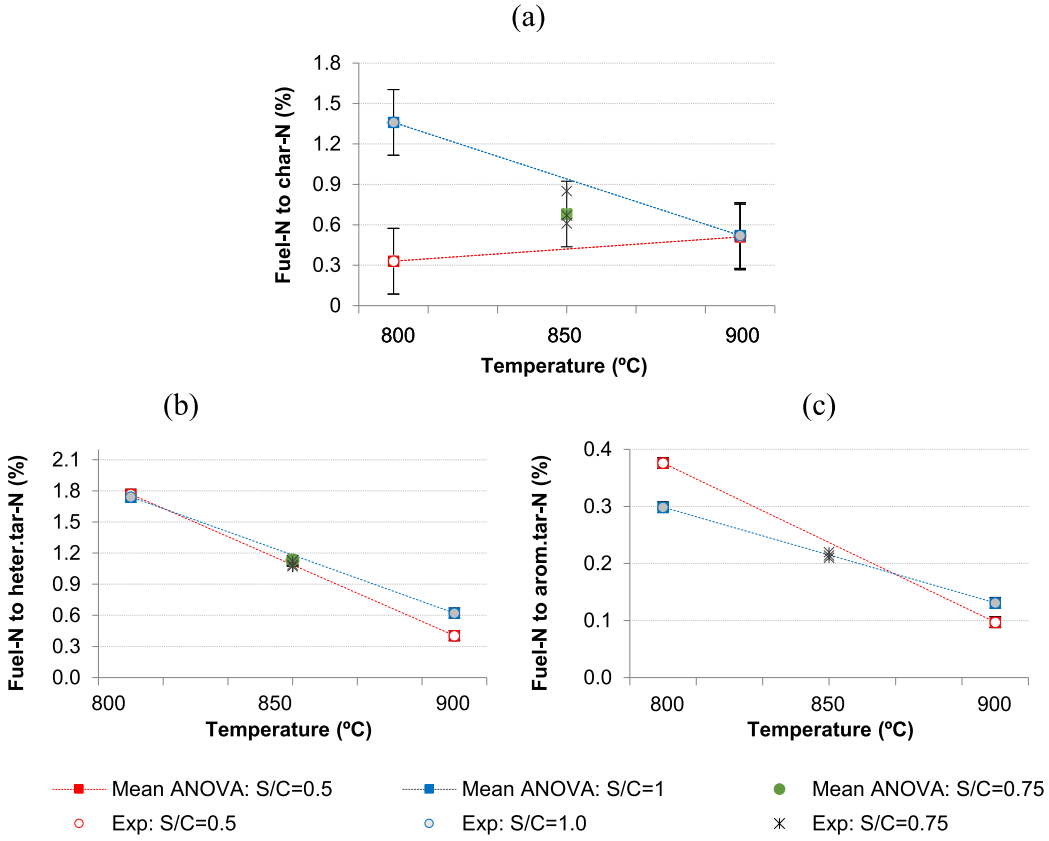

Fig. 4. Effect of temperature and *S/C* mass ratio on the conversion of fuel-N to (a) char-N, (b) heterocyclic tar-N and (c) aromatic tar-N.

The conversions of fuel-N to char-N (<1.5%) obtained in this work were lower than those found by other authors working at similar temperatures but at lower *ER* and without using steam in the mixture of the gasifying agent (Table 1). For instance, Vriesman et al. (2000) obtained significantly higher conversions of fuel-N to char-N when performing the gasification of miscanthus at lower *ER* (0−0.25) and slightly lower temperatures (700−800 °C) (14% at 700 °C and *ER* = 0.16). In summary, the release of nitrogen from char seems to be favored by higher temperatures, higher *ER* and also by the use of steam, which would positively affect the

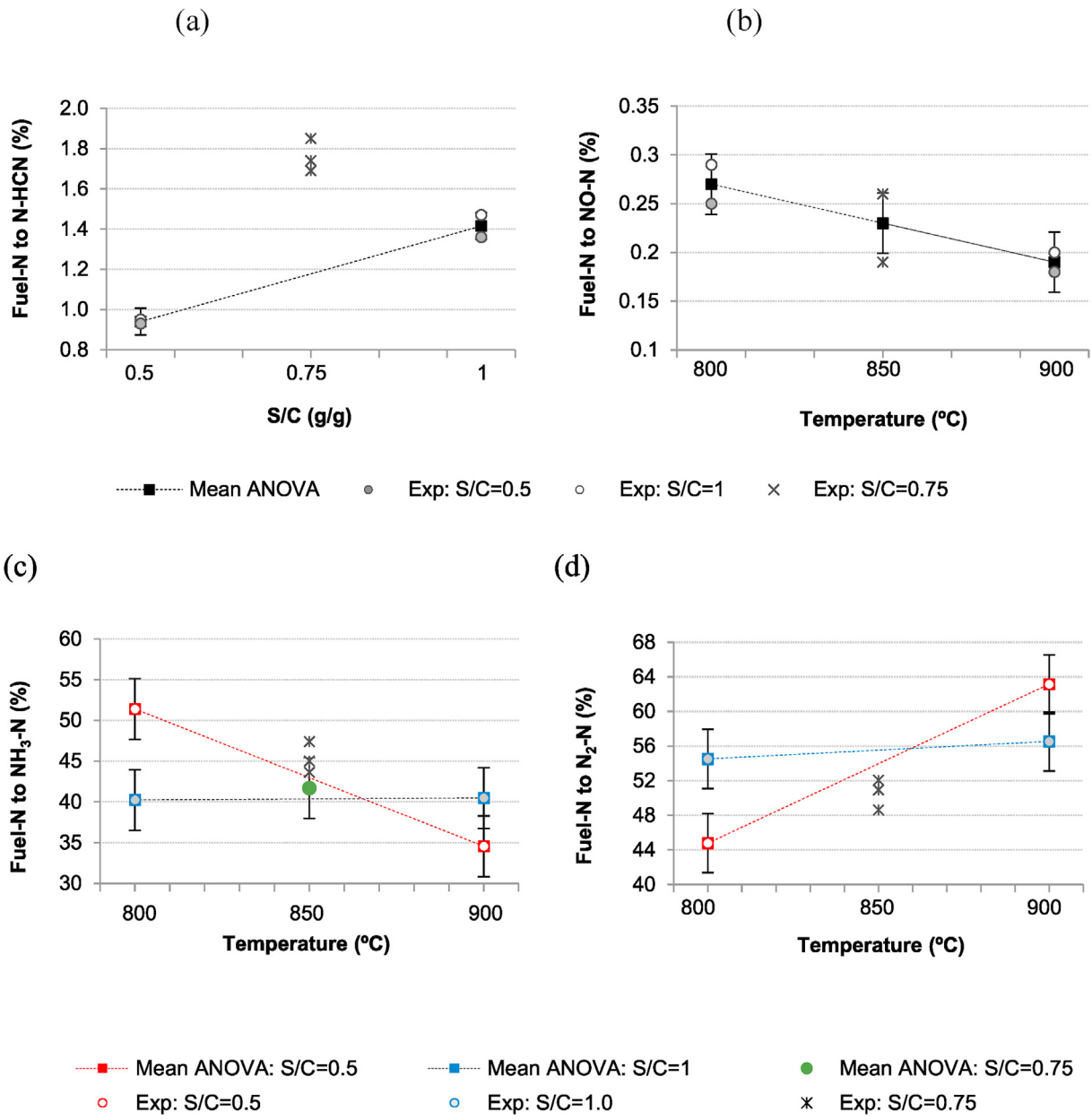

Fig. 5. Effect of temperature and S/C mass ratio on the conversion of fuel-N to (a) HCN–N, (b) NO–N, (c) NH_3–N and (d) N_2–N.

occurrence of devolatilization and char gasification reactions.

On the other hand, the increase in the temperature caused a general decreasing trend in the conversion of fuel-N to heterocyclic tar-N and aromatic tar-N (Fig. 4(b) and (c)), this effect being in both cases more marked when using a *S/C* of 0.5 g g^{-1}. The interaction of the two factors is significant (as shown in Table 5): the effect of the *S/C* ratio on the conversion of fuel-N to both heterocyclic tar-N and aromatic tar-N is different depending on the temperature value. An increase in the *S/C* ratio caused a rise in the conversion of fuel-N to heterocyclic tar-N and aromatic tar-N at the highest *T* studied (900 °C), while it provoked a decrease in the aromatic tar-N yield at the lowest *T* studied (800 °C). The positive effect of the *S/C* ratio on the yield of tar-N compounds at the highest studied temperature is explained by the behavior of both aforementioned N-containing families, but especially because of the evolution of the subfamily pyridinic tar-N, which is the most abundant N-functionality in tar.

During pyrolysis, the char-N functionalities evolve with the temperature. The N-functionality of the raw material (GLU) and of the char coming from its pyrolysis at 900 °C (GLU_PIR900) was analyzed by XPS (see XPS results in the Supplementary Information). The deconvolution of the GLU and GLU_PIR900 N 1s spectra (see Fig. S1) allowed us to determine that the protein-N functionality (401.5 eV) present in the raw GLU evolved mainly to pyridinic-N (400.5 eV) in the GLU-900. Similar N-functionality results were obtained by Wei et al. (2015) when analyzing the evolution of sewage sludge N-functionality during pyrolysis from ambient temperature to 850 °C. Taking into account this functionality of the char-N at high temperatures (pyridinic-N) and the fact that the most abundant class in tar is pyridinic-N, it is thought that a higher *S/C* ratio could promote the formation of this type of compound via char-N gasification reactions (pyridinic char-N (s) + H_2O (g) → pyridinic tar-N (g) + other products) (R1).

The fraction of fuel-N that ended up as tar-N compounds in this work (0.5–2.14%) was lower than in other works (see Table 1). The

higher values found in the literature (5.9–38%) (Aznar et al., 2009; Broer and Brown, 2016) could be attributed to the fact of using an inert bed (sand) in the reactor (not dolomite like in this work) and/or a lower gasification temperature or equivalence ratio than in this work. Detailed results about the fuel-N distribution among the individual N-containing species in tar is provided in Table S5 (Supplementary Information Section).

Fig. 5(a), 5(b), 5(c) and 5(d) show the effect of the *T* and the *S/C* mass ratio on the conversion of fuel-N to the gaseous species HCN–N, NO–N, NH_3–N and N_2–N.

Concerning the conversion of fuel-N to HCN–N (Fig. 5(a)), the *S/C* ratio was the only factor that showed a significant effect (Table 5), increasing this conversion from 0.9 to 1.4% when the *S/C* ratio was augmented from 0.5 to 1.0. It is worth noting that the conversion of fuel-N to HCN–N presented a curvature within the studied intervals of *T* and *S/C*. Regarding the positive effect of steam presence on the yield to HCN, Paterson et al. (2005) also found that steam addition caused a small rise in the HCN concentration during gasification tests with sewage sludge.

Results reported in the literature regarding the fraction of fuel-N that forms HCN show significant variations. As can be observed in Table 1, different studies reported conversions significantly higher (9.8–40%) (Broer and Brown, 2016), lower (<0.2%) (Aljbour and Kawamoto, 2013; Vriesman et al., 2000) and also similar (0.7–1.6%) (Aznar et al., 2009) to those obtained in this work (0.9–1.8%). Some authors have observed that HCN is formed from devolatilization reactions of the fuel-N (Broer and Brown, 2015), as well as during the gasification reactions of fuel-N with steam and during the thermal cracking of volatile-N (Tian et al., 2007). Its formation is also affected by the nitrogen functionality in char (Tian et al., 2014) and by the char reactivity (Tian et al., 2007). On the other hand, HCN is consumed via reactions with H_2 (Cao et al., 2015), H_2O or O_2 (Shimizu et al., 1993). In view of the disparate results found in the literature and the numerous reactions in which HCN takes part, it can be concluded that the conversion of fuel-N to HCN–N is strongly affected by the operating conditions, although some authors have attempted to explain these differences by the use of inadequate sampling methodologies (Broer et al., 2015).

In contrast, the results obtained in this work show that the temperature was the only significant factor in the conversion of fuel-N to NO–N (Fig. 5(b)), showing a slightly negative impact.

Fig. 5(c) and 5(d) show that the effect of the *T* on NH_3–N and N_2–N yields was only significant for the lowest *S/C* studied (0.5 g g^{-1}). While the conversion of fuel-N to NH_3 showed a downward trend with temperature (from 51% at 800 °C to 35% at 900 °C), the effect of *T* on the fuel-N conversion to N_2 was positive (from 45% at 800 °C to 63% at 900 °C). Similar effects of the temperature on the conversion of fuel-N to NH_3–N have been obtained by other authors (Abdoulmoumine et al., 2014; Zhou et al., 2000). Likewise, the effect of the *S/C* ratio was only significant for the lowest *T* studied (800 °C), decreasing the fuel-N conversion to NH_3 from 51% to 40% and increasing the conversion to N_2 when the *S/C* ratio was augmented from 0.5 to 1.0 g g^{-1}. In this regard, Liu and Gibbs (2003) modeled NH_3 emissions obtained in biomass gasification in a fluidized bed and determined that the NH_3 emissions decreased when the moisture of the raw material increased from 10% to 30%.

According to the results shown in the literature, during biomass gasification NH_3 takes part as a product or as a reagent in different stages of the reaction. The results obtained by some authors demonstrate its formation during the pyrolysis stage from biomass-N (Aljbour and Kawamoto, 2013; Broer and Brown, 2015; Vriesman et al., 2000). In the specific case of amino acids, Moldoveanu (2010) pointed to several thermal decomposition reactions of amino acids yielding NH_3. One of these reactions is the thermal fragmentation of the amino acid, giving NH_3, CO_2 and alkenes, as shown for GLU in the following reaction: ($COOH–CH_2–CH_2–CHNH_2–COOH \rightarrow NH_3 + 2CO_2 + CH_3–CH{=}CH_2$; $\Delta H^{\circ}_{298\,K}$ = 166.6 kJ; $\Delta G < 0$ at $T \geq 346$ K; $K_{p,R2}$ (1173 K) = $3.97 \cdot 10^{29}$) (R2). NH_3 can also be thermally released from char-N (Broer and Brown, 2015), and also by gasification reactions with O_2 (Broer and Brown, 2016) or H_2O (Tian et al., 2007). In their biomass gasification model, Liu and Gibbs (2003) proposed some char-N gasification reactions yielding NH_3, which may have also occurred during the gasification experiments carried out in this work: Char-N+$CO_2 \rightarrow NH_3$+products (R3), Char-N+$H_2O \rightarrow NH_3$+products (R4) and Char-N+$H_2 \rightarrow NH_3$+products (R5). The cracking and reforming reactions of tar-N compounds as a source of NH_3 have also been proved by the results found by other authors (Broer and Brown, 2015; Tian et al., 2007). On the other hand, NH_3 also takes part in secondary gas-phase reactions, either as a product or as a reagent (Liu and Gibbs, 2003), although under gasification conditions the gas-phase-reactions leading to the disappearance of NH_3 are predominant. In these secondary gas-phase reactions, NH_3 likely disappears as a result of reactions with radicals to form NH_2, which may undergo further decomposition to give N_2 and H_2, giving as a global reaction (2 NH_3 (g) ↔ N_2 (g) + 3 H_2 (g); $\Delta H^{\circ}_{298\,K}$ = 92.38 kJ; $\Delta G < 0$ at $T \geq 462$ K) (R6), which is shifted to the product side for temperatures greater than 462 K). Another gas-phase route that could lead to the loss of NH_3 may be its partial oxidation under reducing conditions (NH_3 (g) + ¾ O_2(g) ↔ 1/2N_2 (g) + 3/2 H_2O (g); $\Delta H^{\circ}_{298\,K}$ = −316.54 kJ; $\Delta S^{\circ}_{298\,K}$ = 32.7 J K^{-1}; $\Delta G < 0$ at any temperature) (R7).

Both NH_3 formation and consuming reactions may be affected by the operating conditions studied. The final NH_3 yield (measured at the gasifier exit) depends on the overall effect of the reactions related to the N chemistry (many of them summarized above). In the case of temperature, it is assumed that if char-N gasification reactions and tar-N cracking and reforming reactions behave in the same way as those involving non-heteroatom char and tar, they would be favored by an increase in temperature. At the temperatures studied, the aforementioned NH_3 consuming reactions (R6 and R7) are completely shifted to the products side ($K_{p,R6}$ (1173 K) = $8.1 \cdot 10^6$ and ($K_{p,R7}$ (1173 K) = $3.6 \cdot 10^{15}$), although R6 is more likely to occur to a greater extent due to its lower activation energy (Monnery et al., 2001). The observed decrease in the yield of NH_3 with the increase in the *S/C* ratio at 800 °C could be related to the higher availability of O_2 (higher *ER*) linked to the highest *S/C* ratio, which could promote the consuming of NH_3 via R7. The chemical reactions used in the discussion of the results and their thermodynamic and kinetic parameters are listed in Table S6.

Some of the values found in the literature for the conversion of fuel-N to NH_3–N and N_2–N (see Table 1) are in consonance with those found in this work (see Tables 3 and 6). As a general rule, at a low equivalence ratio or at low temperatures the joint yield of HCN–N, tar-N and char-N are high, while the yield of NH_3 is not usually high (Aznar et al., 2009; Broer and Brown, 2016; Vriesman et al., 2000). However, if the equivalence ratio and/or the gasification temperature are sufficiently high, then a significant high yield of NH_3 can be obtained (Jeremias et al., 2014; Zhou et al., 2000), unless it is reduced in favor of N_2 production through R6 (Aznar et al., 2009; Zhou et al., 2000). As discussed previously, the main origin of the N_2 produced from fuel-N is the NH_3 decomposition reaction (R6). The conversions of fuel-N to N_2–N obtained in this work and reported in literature highlight that, under gasification operating conditions, this reaction (R6) does not reach thermodynamic equilibrium, since the obtained experimental concentrations are usually far from the ones calculated for the thermodynamic equilibrium at gasification temperature ranges (for example:

$y_{N2} = 0.24997$, $y_{H2} = 0.74992$, $y_{NH3} = 0.011$ at 1100 K and 1 atm). The different extent of this gas-phase reaction, in which thermodynamic factors (such as temperature and pressure) and kinetic factors (such as residence time, temperature or catalysis) play a significant role, will be decisive in the final yields of NH_3 and N_2. In fact, the effect that pressure exerts on the thermodynamics of the NH_3 decomposition reaction (R6) was evidenced by the results reported by de Jong et al. (2003) when studied the gasification of miscanthus in a pressurized fluidized bed (0.4–0.7 MPa). In that work, they obtained higher conversions to NH_3–N (94–95%) than those at atmospheric pressure, which shows the shifting of the equilibrium composition to the reagents side as the pressure increases.

Usually, the thermodynamic equilibrium composition is not reached during the pyrolysis or gasification of a N-containing raw material, but experimental data in the literature reveal that the decomposition of NH_3 into N_2 tends to occur to a certain extent even at very short gas residence times (around 1 s) (Broer and Brown, 2015). When studying the pyrolysis of switchgrass at temperatures between 650 and 850 °C, these authors reported fuel-N conversions to N_2 between 7 and 35% when working at short residence times of 1.0–1.2 s. Therefore, the effect of the residence time will be a determining factor in the final fuel-N distribution between NH_3 and N_2.

According to the results obtained in this work, the highest yield of NH_3–N from GLU gasification has been obtained at the lowest *T* studied (800 °C) and at the lowest *S/C* ratio (0.5). Moreover, it can be stated that the enhancing effect of the temperature on the NH_3 decomposition reaction outweighs its positive effect on the reactions involved in its formation (final negative effect of temperature on the net production of NH_3). Lastly, taking into account the general fuel-N distribution obtained, it can be said that, under the operating conditions studied, the disfavoring of the decomposition of NH_3 into N_2 (R6) is of utmost importance to achieve a high conversion to NH_3.

3.2. Gasification of N-rich biological residues

The first part of the experimental work in this study used GLU as a model compound for obtaining a first approach to evaluating the influence of the *T* and the *S/C* ratio on the fuel-N distribution during the gasification process. In order to complete the study, some gasification experiments with real N-rich biological residues, such as SS and MBM, were carried out in the same experimental setup under selected operating conditions. Table 6 summarizes the operating conditions and the main results of these experiments. The fuel-N yields to the different N-containing products have been calculated taking the fraction of fuel-N as a basis, but also the specific fraction of protein-fuel-N (see section 2.1.1).

In spite of the disparity on the amino acid composition of the three raw materials (pure GLU, SS and MBM, see Fig. 1), similar general fuel-N distributions, with char-N, tar-N, NO, and HCN as minority products and NH_3 and N_2 as the majority ones, were obtained from their gasification. However, if the fuel-N distribution into these minority products is analyzed in greater depth, significant differences can be found among the raw materials: tar-N accounted for the highest fraction of fuel-N (2.14%) in the case of GLU, NO–N (0.61%) in the case of SS, char-N (2.6%) in the case of MBM at 800 °C and tar-N (0.79%) in the case of MBM at 900 °C.

The fuel-N distribution obtained in some of the works shown in Table 1 (Jeremias et al., 2014; Schweitzer et al., 2018; Zhou et al., 2000) is similar to that obtained in this work, in which a low joint yield to char-N, tar-N, HCN–N and NO–N over fuel-N was obtained, while NH_3–N and N_2–N accounted for the highest fuel-N fraction. In other works, higher conversions of fuel-N to tar-N (Aznar et al., 2009; Broer and Brown, 2016) and char-N (Broer and Brown, 2016; Vriesman et al., 2000) have been reported. The higher conversions of fuel-N to tar-N obtained in literature works could be related with the low ER, the low temperature, and with the fact that in these works neither dolomite nor steam were used.

Tar compounds generated in the gasification of SS and MBM were analyzed by GC-MS/FID. A greater number of tar compounds were identified in the condensates obtained from the gasification of both residues than in those obtained from GLU (see Tables S4, S7 and S8). Apart from the three chemical families appearing in GLU tar (heterocyclic tar-N (1), aromatic tar-N (2) and PAH (3)), compounds belonging to two other chemical families (without containing N) were detected: O-containing tar (4) and other heteroatomic containing tar (5). The mass percentage of N-containing tar over total tar was higher in the case of GLU (76–93 wt % of tar compounds contained N) than for the residues (42–54 wt % of tar compounds contained N). The PAH-tar fraction in the tar coming from the residues was significantly higher than in the tar coming from GLU. The higher proportion of PAH-tar and the presence of the other two chemical families of compounds is due to the existence of other constituents apart from the N-protein fraction in the residues, which also generate tar during gasification.

Regarding N-containing tar families and subfamilies, heterocyclic tar-N accounted for between 46% and 65% of the tar-N in the case of the residues, while it was around 83–85% when coming from GLU both at 800 and at 900 °C. The fraction of aromatic tar-N (over total tar-N) generated from the residues (15–30%) seems to be slightly higher than that generated from GLU under the same operating conditions (6–18%). As previously mentioned, pyridines were the most abundant compounds among the heterocyclic tar-N obtained in GLU gasification. In the case of MBM, three chemical families were the most abundant: pyridines, nitriles and quinolines. Nitriles stand out from the rest of the families in the SS tar compounds because of their higher proportion. The origin of aromatic nitriles could be the cyclization of fatty nitriles, which are typical compounds generated during the pyrolysis of SS as a consequence of the gas phase reaction between fatty acids and NH_3 released during the pyrolysis stage (Fonts et al., 2017).

The fractions of protein-fuel-N that ended up as NH_3 in the case of SS gasified at 800 °C (41%) and MBM gasified at 900 °C (44%) were slightly lower than that obtained when GLU was gasified at 800 °C (51%). A similar conversion rate of protein fuel-N into NH_3–N (48%) was reported by Schweitzer et al. (2018) for the steam gasification of SS (7.1 wt % N, daf basis) at 800 °C, using a *S/C* molar ratio of 1.5 and silica sand as bed material. When MBM was gasified at 800 °C, a significant increase in the yield of NH_3–N over protein-fuel-N (86%) was observed. The presence of iron-containing minerals, greater in the case of SS than in MBM (see Table 2), could also have a catalytic effect promoting the decomposition of NH_3 into N_2 and H_2 (Chen et al., 2011), explaining the reduced production of NH_3 from SS in comparison with GLU or MBM. The higher yield of NH_3–N obtained from MBM than from GLU under the same operating conditions (800 °C and $S/C = 0.5$ g g^{-1}) could be related to the high content of calcium-containing minerals present in MBM (see Table 2). According to Wei et al. (2018), calcium-containing minerals promote the conversion of protein-N in NH_3 during pyrolysis. The decrease in the yield of NH_3–N with *T* observed in the experiments carried out with MBM matches with the *T* effect observed for the NH_3–N yield in the GLU gasification experiments.

In conclusion, a comparison of these experimental data has shown that although the fuel-N distribution is affected by the raw material used, the general distribution of majority N-containing products (NH_3 and N_2) and minority N-containing products (HCN, NO, tar-N and char-N) remains similar independently of the raw material. In the same way, the decreasing NH_3–N yield with *T*

Table 6
Operating conditions and results of the gasification of SS and MBM.

	Tests 8, 9	Test 10	Test 11
Raw material	SS	MBM	MBM
Average gasification temperature (°C)	800	800	900
Steam-to-carbon ($g \cdot g^{-1}$)	0.5	0.5	0.5
Average gas residence time, s [(a)]	7.2 ± 0.3	8.1	5.0
Tar yield (g tar·kg^{-1} fed GLU)			
Total tar (1 + 2+3 + 4+5)	4.5 ± 0.1	6.4	11.7
Total N-containing tar (1 + 2)	2.0 ± 0.2	2.7	6.2
Heterocyclic-N tar (1)	0.93 ± 0.05	1.8	2.8
Aromatic-N tar (2)	1.1 ± 0.1	1.0	3.4
PAH tar (3)	2.28 ± 0.09	3.6	5.1
O-containing tar (without N) (4)	0.09 ± 0.02	0.026	0.21
Heteroatomic-containing tar (without neither N nor O) (5)	0.11 ± 0.03	0.071	0.06
Fraction of N-containing tar in total tar (wt. %)	45 ± 2	42	54
Fuel-N distribution, (% over fuel-N)/(% over protein-fuel-N)			
NH_3—N	30/41 ± 1	67/86	34/44
HCN—N	0.451/0.617 ± 0.006	0.823/1.05	0.322/0.413
NO—N	0.61/0.83 ± 0.02	0.49/0.63	0.75/0.96
Tar-N (Total, 1 + 2)	0.54/0.74 ± 0.05	0.37/0.47	0.79/1.01
Fuel-N to heterocyclic tar-N (1)	0.25/0.43 ± 0.01	0.24/0.31	0.38/0.484
Fuel-N to pyridinic-N (1-a)	0.066/0.090	0.14/0.18	0.17/0.2
Fuel-N to pyrrolic-N (1-b)	0.034/0.047	0.0003/0.0004	0.036/0.046
Fuel-N to quinolinic-N (1-c)	0.075/0.10	0.055/0.070	0.096/0.12
Fuel-N to indoles-N (1-d)	0.077/0.11	0.040/0.051	0.080/0.10
Fuel-N to indolizines-N (1-e)	0	0	0.0081/0.0111
Fuel-N to aromatic tar-N (2)	0.29/0.40	0.13/0.17	0.40/0.52
Fuel-N to aromatic nitriles-N (2-f)	0.27/0.37	0.07/0.09	0.39/0.50
Fuel-N to aromatic azides and amines-N (2-g)	0.02/0.03	0.06/0.08	0.01/0.02
Char-N	0.5/0.7	2.6/3.3	0.36/0.46
N—N_2 (by difference)	68/55 ± 1	28/8	64/53
NH_3 yield (kg $NH_3 \cdot ton^{-1}$ residue)	17.05 ± 0.08	81.0	40.8
Syngas production (m^3(STP)$\cdot kg^{-1}$ residue)	1.67 ± 0.03	2.51	2.48
Gas lower heating value (MJ$\cdot m^{-3}$(STP) syngas) [(b)]	2.7 ± 0.2	3.29	3.19
Power generation (GJ$\cdot ton^{-1}$ NH_3)	262 ± 3	102	194

[a] The residence time of gases and vapors in the reactor was calculated from the reactor volume and the gas flow data (including steam and tar vapors).
[b] Calculated from the syngas composition determined with the micro gas chromatograph (Agilent 3000-A).

observed in the GLU gasification experiments was corroborated when MBM was gasified at 800 and 900 °C.

As commented in the "Introduction Section", the alternatives in the literature to the conventional Haber-Bosch synthesis provide more favorable energy performance thanks to the integration with renewable energy sources, even reaching net power production in some of them such as the one based on syngas chemical looping for the production of pure H_2, N_2 and power (Nurdiawati et al., 2019). Against the alternatives from the literature, the process proposed in the present work could produce directly NH_3 from the own autothermal gasification of N-rich biological residues without integrating an energy supplier process, gaining even higher energy efficiency thanks to the syngas combustion. Taking into account the yield of NH_3 as well as the syngas production and the gas lower heating value (see Table 6), the combustion of the syngas generated from SS and MBM could produce between 102 and 262 GJ ton^{-1} NH_3, turning the NH_3 synthesis from an energy demanding process (28 GJ ton^{-1} NH_3 required for the best existing industrial plants (Rafiqul et al., 2005)) into a power-producing one. Apart from this, another environmental advantage of this process is the use of a reactive-N source instead of the stable atmospheric N_2, contributing to balance the nitrogen biogeochemical cycle. N_2 from atmosphere, used in the other alternatives as source of N for NH_3 synthesis, is literally unlimited, not happening the same for N-rich biological residues. Taking into account the aforementioned generation of these two N-rich biological residues in the EU and the conversions of fuel-N to NH_3—N obtained, the process proposed in this work could produce around 10% of the NH_3—N produced currently in the EU (13.5 million tons) (Eurostat, 2020) (see the Supplementary Information Section). The increase in the conversion of fuel-N to NH_3—N, as well as the use of other sources of reactive-N, such as livestock manure or N-containing thermostable polymers, would contribute to increase this production share.

4. Conclusions

A sustainable route for the production of NH_3 has been proposed in this work via autothermal gasification of N-rich biological residues, thereby recycling and converting the reactive nitrogen and the hydrogen contained in these residues into NH_3 and enabling their valorization.

The parametric study carried out with a model amino acid compound (glutamic acid: GLU) revealed that the temperature (800—900 °C) affected the fuel-N distribution more significantly than the steam-to-carbon (*S/C*) mass ratio (0.5—1.0 g g^{-1}). The temperature had a negative effect on the conversion of fuel-N to char-N, heterocyclic tar-N, aromatic tar-N and NH_3—N, while it had a positive effect on the conversion to N_2. The increase in the *S/C* ratio had a positive impact on the yield to N-containing tar compounds, mainly pyridinic tar- N, as well as a negative impact on NH_3 production when operating at 800 °C.

Under all the operating conditions and raw materials studied (pure GLU, sewage sludge: SS or meat and bone meal: MBM), a very small fraction of fuel-N was lost in the form of char-N, tar-N, HCN—N and NO—N (joint yields between 2.1 and 5.2% of fuel-N), while NH_3 and N_2 were the most abundant N-containing products. Similar general fuel-N distributions were obtained from the gasification of the three raw materials despite their different amino acid composition. Although the joint yields of N_2 and NH_3 are

expected to be the most abundant among the N-containing products, its individual yields were significantly affected by the extent of the NH_3 decomposition reaction, which in turns depends on the temperature, the gas residence time and the metals present in the raw materials. The MBM gasification experiments confirmed the negative effect of the temperature on the fuel-N conversion into NH_3–N that was determined in the GLU experiments. The different conversion values of fuel-N into NH_3–N obtained from the real residues (30% for SS and 67% for MBM) and that obtained from GLU (51%) were attributed to the effect of the metals present in the residues. The iron-containing minerals of SS would favor the decomposition of NH_3 into N_2, while the calcium-containing minerals of MBM would disfavor this decomposition reaction and favor the conversion of protein-N into NH_3. The optimization of the operating conditions to be used with each raw material, particularly the gasification temperature, is critical to maximize NH_3 production.

Around 10% of the NH_3 produced annually in the EU could be produced by the process proposed in this work, which involves the recycling of the nitrogen and the hydrogen contained in SS and MBM via autothermal gasification. This process is also promising for achieving net energy production thanks to the combustion of the syngas generated (102–262 $GJ \cdot ton^{-1}$ NH_3).

Funding

The authors thank the Aragon Government and the European Social Fund (GPT group, T22-20R), and the MINECO (Research Project CTQ 2015-72475-EXP) for financial support.

CRediT authorship contribution statement

Noemí Gil-Lalaguna: Methodology, Validation, Conceptualization, Methodology, Formal analysis, Investigation, Resources, Data curation, Writing - original draft, Writing - review & editing, Visualization. **Zainab Afailal:** Investigation. **María Aznar:** Methodology, Writing - review & editing. **Isabel Fonts:** Conceptualization, Methodology, Formal analysis, Resources, Data curation, Writing - original draft, Writing - review & editing, Visualization, Project administration, Funding acquisition.

Declaration of competing interest

The authors declare that they have no known competing financial interests or personal relationships that could have appeared to influence the work reported in this paper.

Appendix A. Supplementary data

Supplementary data to this article can be found online at https://doi.org/10.1016/j.jclepro.2020.124417.

References

Abdoulmoumine, N., Kulkarni, A., Adhikari, S., 2014. Effects of temperature and equivalence ratio on pine syngas primary gases and contaminants in a bench-scale fluidized bed gasifier. Ind. Eng. Chem. Res. 53 (14), 5767–5777.

Aljbour, S.H., Kawamoto, K., 2013. Bench-scale gasification of cedar wood – Part II: effect of Operational conditions on contaminant release. Chemosphere 90 (4), 1501–1507.

Andersson, Jim, Lundgren, Joakin, 2014. Techno-economic analysis of ammonia production via integrated biomass gasification. Appl. Energy.

Aznar, M., San Anselmo, M., Manya, J.J., Benita Murillo, M., 2009. Experimental study examining the evolution of nitrogen compounds during the gasification of dried sewage sludge. Energy Fuels 23, 3236–3245.

Baltrusaitis, J., 2017. Sustainable ammonia production. ACS Sustain. Chem. Eng. 5 (11), 9527-9527.

Boerner, L.K., 2019. Industrial ammonia production emits more CO_2 than any other chemical-making reaction. Chemists want to change that. Chem. Eng. News 97 (24), 18–22.

Broer, K.M., Brown, R.C., 2015. The role of char and tar in determining the gas-phase partitioning of nitrogen during biomass gasification. Appl. Energy 158, 474–483.

Broer, K.M., Brown, R.C., 2016. Effect of equivalence ratio on partitioning of nitrogen during biomass gasification. Energy Fuels 30 (1), 407–413.

Broer, K.M., Woolcock, P.J., Johnston, P.A., Brown, R.C., 2015. Steam/oxygen gasification system for the production of clean syngas from switchgrass. Fuel 140, 282–292.

Brunning, A., 2019. Periodic graphics: environmental impact of industrial reactions. Chem. Eng. News 97 (24), 23.

Cao, J.P., Huang, X., Zhao, X.Y., Wei, X.Y., Takarada, T., 2015. Nitrogen transformation during gasification of livestock compost over transition metal and Ca-based catalysts. Fuel 140, 477–483.

Corella, J., Toledo, J.M., Padilla, R., 2004. Olivine or dolomite as in-bed additive in biomass gasification with air in a fluidized bed: which is better? Energy Fuels 18 (3), 713–720.

Cui, X., Tang, C., Zhang, Q., 2018. A review of electrocatalytic reduction of dinitrogen to ammonia under ambient conditions. Advanced Energy Materials 8 (22), 1800369.

Chang, L., Xie, Z., Xie, K.-C., Pratt, K.C., Hayashi, J.-i., Chiba, T., Li, C.-Z., 2003. Formation of NOx precursors during the pyrolysis of coal and biomass. Part VI. Effects of gas atmosphere on the formation of NH3 and HCN. Fuel 82 (10), 1159–1166.

Chen, H., Namioka, T., Yoshikawa, K., 2011. Characteristics of tar, NOx precursors and their absorption performance with different scrubbing solvents during the pyrolysis of sewage sludge. Appl. Energy 88 (12), 5032–5041.

de Jong, W., Ünal, Ö., Andries, J., Hein, K.R.G., Spliethoff, H., 2003. Thermochemical conversion of brown coal and biomass in a pressurised fluidised bed gasifier with hot gas filtration using ceramic channel filters: measurements and gasifier modelling. Appl. Energy 74 (3), 425–437.

Eurostat, 2019. Sewage Sludge Production and Disposal. www.ec.europa.eu/eurostat/web/environment/water. Accessed 31/01/2020.

Eurostat, 2020. Production of NH3-N in EU (28 Countries) in 2018. www.ec.europa.eu/eurostat/web/prodcom/data/database?p_p_id=NavTreeportletprod_WAR_NavTreeportletprod_INSTANCE_iSpjsGQt409q&p_p_lifecycle=0&p_p_state=normal&p_p_mode=view&p_p_col_id=column-2&p_p_col_count=1. Accessed 14/04/2020.

Fonts, I., Juan, A., Gea, G., Murillo, M.B., Sanchez, J.L., 2008. Sewage sludge pyrolysis in fluidized bed, 1: influence of operational conditions on the product distribution. Ind. Eng. Chem. Res. 47 (15), 5376–5385.

Fonts, I., Navarro-Puyuelo, A., Ruiz-Gomez, N., Atienza-Martinez, M., Wisniewsky, A., Gea, G., 2017. Assessment of the production of value-added chemical compounds from sewage sludge pyrolysis liquids. Energy Technol. 5 (1), 151–171.

Gálvez, M.E., Frei, A., Meier, F., Steinfeld, A., 2009. Production of AlN by carbothermal and methanothermal reduction of Al_2O_3 in a N_2 flow using concentrated thermal radiation. Ind. Eng. Chem. Res. 48 (1), 528–533.

Gil-Lalaguna, N., Sánchez, J.L., Murillo, M.B., Rodríguez, E., Gea, G., 2014. Air-steam gasification of sewage sludge in a fluidized bed. Influence of some operating conditions. Chem. Eng. J. 248, 373–382.

Hansson, K.-M., Samuelsson, J., Tullin, C., Åmand, L.-E., 2004. Formation of HNCO, HCN, and NH3 from the pyrolysis of bark and nitrogen-containing model compounds. Combust. Flame 137 (3), 265–277.

Jędrejek, D., Levic, J., Wallace, J., Oleszek, W., 2016. Animal by-products for feed: characteristics, European regulatory framework, and potential impacts on human and animal health and the environment. J. Anim. Feed Sci. 25 (3), 189–202.

Jeremias, M., Pohorely, M., Bode, P., Skoblia, S., Beno, Z., Svoboda, K., 2014. Ammonia yield from gasification of biomass and coal in fluidized bed reactor. Fuel 117, 917–925.

Jorgensen, A.D., Picel, K.C., Stamoudis, V.C., 1990. Prediction of gas chromatography flame ionization detector response factors from molecular structures. Anal. Chem. 62 (7), 683–689.

Juangsa, F.B., Aziz, M., 2019. Integrated system of thermochemical cycle of ammonia, nitrogen production, and power generation. Int. J. Hydrogen Energy 44 (33), 17525–17534.

Kurkela, E., Stahlberg, P., 1992. Air gasification of peat, wood and Brown coal in a pressurized fluidized bed reactor. 2. Formation of nitrogen-compounds. Fuel process. Technol. 31 (1), 23–32.

Leppalahti, J., Koljonen, T., 1995. Nitrogen evolution from coal, peat and wood during gasification - literature review. Fuel Process. Technol. 43 (1), 1–45.

Liu, H., Gibbs, B.M., 2003. Modeling NH_3 and HCN emissions from biomass circulating fluidized bed gasifiers. Fuel 82 (13), 1591–1604.

Michalsky, R., Pfromm, P.H., 2011. Chromium as reactant for solar thermochemical synthesis of ammonia from steam, nitrogen, and biomass at atmospheric pressure. Sol. Energy 85 (11), 2642–2654.

Moldoveanu, S.C., 2010. Pyrolysis of organic molecules with applications to health and environmental issues. In: Moldoveanu, S.C. (Ed.), Techniques and Instrumentation in Analytical Chemistry. Elsevier, p. 724.

Monnery, W.D., Hawboldt, K.A., Pollock, A.E., Svrcek, W.Y., 2001. Ammonia pyrolysis and oxidation in the claus furnace. Ind. Eng. Chem. Res. 40 (1), 144–151.

Nurdiawati, A., Zaini, I.N., Amin, M., Sasongko, D., Aziz, M., 2019. Microalgae-based coproduction of ammonia and power employing chemical looping process. Chem. Eng. Res. Des. 146, 311–323.

Paterson, N., Zhuo, Y., Dugwell, D., Kandiyoti, R., 2005. formation of hydrogen cyanide and ammonia during the gasification of sewage sludge and bituminous coal. Energy Fuels 19 (3), 1016–1022.

Patil, B.S., Wang, Q., Hessel, V., Lang, J., 2015. Plasma N_2-fixation: 1900–2014. Catal. Today 256, 49–66.

Qiao, L., Duan, G, Zhang, S, Ren, Y, Sun, Y, Tang, Y, Wan, P, Pang, R, Chen, Y, Rusell, A.G, Fan, M, 2020. Electrochemical ammonia synthesis catalyzed with a CoFe layered double hydroxide – A new initiative in clean fuel synthesis. J. Clean. Prod. 250. In press.

Rafiqul, I., Weber, C., Lehmann, B., Voss, A., 2005. Energy efficiency improvements in ammonia production—perspectives and uncertainties. Energy 30 (13), 2487–2504.

Ren, Q., Zhao, C., 2015. Evolution of fuel-N in gas phase during biomass pyrolysis. Renew. Sustain. Energy Rev. 50, 408–418.

Rockström, J., Sachs, J.D., Öhman, M.C., Schmidt-Traub, G., 2013. Sustainable development and planetary boundaries. In: Background Paper for the High-Level Panel of Eminent Persons on the Post-2015 Development Agenda, p. 45 (United Nations).

Rockström, J., Steffen, W., Noone, K., Persson, Å., Chapin III, F.S., Lambin, E., Lenton, T.M., Scheffer, M., Folke, C., Schellnhuber, H.J., Nykvist, B., de Wit, C.A., Hughes, T., van der Leeuw, S., Rodhe, H., Sörlin, S., Snyder, P.K., Costanza, R., Svedin, U., Falkenmark, M., Karlberg, L., Corell, R.W., Fabry, V.J., Hansen, J., Walker, B., Liverman, D., Richardson, K., Crutzen, P., Foley, J., 2009a. Planetary boundaries: exploring the safe operating space for humanity. Ecol. Soc. 14 (2).

Rockström, J., Steffen, W., Noone, K., Persson, A., Chapin III, F.S., Lambin, E.F., Lenton, T.M., Scheffer, M., Folke, C., Schellnhuber, H.J., Nykvist, B., de Wit, C.A., Hughes, T., van der Leeuw, S., Rodhe, H., Sorlin, S., Snyder, P.K., Costanza, R., Svedin, U., Falkenmark, M., Karlberg, L., Corell, R.W., Fabry, V.J., Hansen, J., Walker, B., Liverman, D., Richardson, K., Crutzen, P., Foley, J.A., 2009b. A safe operating space for humanity. Nature 461 (7263), 472–475.

Scanlon, J.T., Willis, D.E., 1985. Calculation of flame ionization detector relative response factors using the effective carbon number concept. J. Chromatogr. Sci. 23 (8), 333–340.

Schweitzer, D., Gredinger, A., Schmid, M., Waizmann, G., Beirow, M., Spörl, R., Scheffknecht, G., 2018. Steam gasification of wood pellets, sewage sludge and manure: gasification performance and concentration of impurities. Biomass Bioenergy 111, 308–319.

Shimizu, T., Ishizu, K., Kobayashi, S., Kimura, S., Shimizu, T., Inagaki, M., 1993. Hydrolysis and oxidation of hydrogen cyanide over limestone under fluidized bed combustion conditions. Energy Fuels 7 (5), 645–647.

Tian, F.-J., Yu, J., McKenzie, L.J., Hayashi, J.-i., Li, C.-Z., 2007. Conversion of fuel-N into HCN and NH_3 during the pyrolysis and gasification in steam: a comparative study of coal and biomass. Energy Fuels 21 (2), 517–521.

Tian, K., Liu, W.-J., Qian, T.-T., Jiang, H., Yu, H.-Q., 2014. Investigation on the evolution of N-containing organic compounds during pyrolysis of sewage sludge. Environ. Sci. Technol. 48 (18), 10888–10896.

U.S.G.S., 2018. Mineral Commodity Summaries. U.S. Department of the Interior, U.S. Geological Survey., Reston, Virginia, p. 117. https://doi.org/10.3133/70194932.

Vriesman, P., Heginuz, E., Sjostrom, K., 2000. Biomass gasification in a laboratory-scale AFBG: influence of the location of the feeding point on the fuel-N conversion. Fuel 79 (11), 1371–1378.

Wang, L., Xia, M., Wang, H., Huang, K., Qian, C., Maravelias, C.T., Ozin, G.A., 2018. Greening ammonia toward the solar ammonia refinery. Joule 2 (6), 1055–1074.

Wei, L., Liu, M., Liang, F., Yang, T., Wen, L., 2018. Effects of CaO on nitrogen transformation during pyrolysis of soybean protein. Energy Sources, Part A Recovery, Util. Environ. Eff. 40 (22), 2641–2647.

Wei, L., Wen, L., Yang, T., Zhang, N., 2015. Nitrogen transformation during sewage sludge pyrolysis. Energy Fuels 29 (8), 5088–5094.

Yu, Q.Z., Brage, C., Chen, G.X., Sjostrom, K., 2007. The fate of fuel-nitrogen during gasification of biomass in a pressurised fluidised bed gasifier. Fuel 86 (4), 611–618.

Zhou, J., Masutani, S.M., Ishimura, D.M., Turn, S.Q., Kinoshita, C.M., 2000. Release of fuel-bound nitrogen during biomass gasification. Ind. Eng. Chem. Res. 39 (3), 626–634.